ORIGINAL ARTICLE

Study on high-speed vibration cutting of titanium alloy considering cutting edge radii

Xu Zhang[1] · Yaotian Cheng[1] · Mingqiang Lv[1] · Xuchao Miao[1] · Chaoyu Xie[1]

Abstract

Ultrasonic vibration cutting (UVC) is an advanced machining method used to improve machining performance and surface quality in the manufacturing industry. However, the separation characteristic disappears when the cutting speed exceeds the maximum vibration speed, which limits its wide application in high-speed machining. Therefore, this study used the finite element method (FEM) to study the high-speed vibration cutting (HVC) processing performance of titanium alloys. High-speed vibration cutting is a precision machining method with a smaller cutting depth and feed rate, so it is necessary to consider the influence of the cutting edge radii on the cutting process. The cutting edge radii on high-speed vibration cutting and the impact of the traditional cutting process are discussed. The results show that the change in the minimum uncut chip thickness caused by changing the cutting edge radii during precision cutting has a significant influence on the experimental results. In addition, a simulation model was established, and comprehensive numerical analysis and comparison of high-speed vibration cutting, ultrasonic vibration cutting, and conventional cutting (CC) were performed to tool wear, cutting temperature, cutting force, and stress distribution. The simulation results indicate that the tool wear depth of traditional cutting during high-speed cutting is up to three times that of high-speed vibration cutting. High-speed vibration cutting weakens the influence of the cutting edge radii, but this new vibration cutting method did not significantly reduce the cutting temperature under dry cutting conditions.

1 Introduction

Nowadays, Ti6Al4V titanium alloys are commonly utilized in medical instruments, ocean engineering, and the aircraft industry, owing to their good corrosion resistance, high specific strength, and high heat resistance. Titanium alloys, on the other hand, produce a lot of cutting heat during machining and are attached to the tool/chip interface, resulting in a shorter tool life but also affecting the quality of the processed surface owing to their active chemical properties and poor thermal conductivity.

In the past few decades, difficult-to-process materials like nickel-chromium and titanium alloys have attracted the attention of many manufacturing scientists and engineers. A series of advanced machining methods have been proposed, such as ultrasonic vibration machining, micro-cutting, and heat-assisted machining. Zhu et al. [1] revealed the effect of micro-texture surface characteristics on the tribological properties of processed surfaces during ultrasonic vibration-assisted milling; Microtexture under ultrasonic vibration has a significant effect on improving frictional and wear performance by reducing the coefficient of friction and its fluctuations, according to experimental results. Zheng et al. [2] analyzed the experimental results of conventional milling (CM) and ultrasonic vibration-assisted milling (UVAM) of titanium alloys, and found that under high-frequency vibration, the uniformity and consistency of the workpiece surface texture were significantly improved; However, under dry processing conditions, there was no substantial change in the surface tribological properties between CM and UVAM processing. Ni et al. [3] introduced minimum quantity lubrication (MQL) in ultrasonic vibration-assisted milling, and analyzed conventional milling, UVAM, and UVAM & MQL processing methods. The results showed that they are

✉ Yaotian Cheng
  17602173791@163.com

1 School of Mechanical and Automotive Engineering,
   Shanghai University of Engineering Science,
   Shanghai 201620, China

comparable to CM and traditional UVAM. In contrast, the feed-direction UVAM & MQL methods have an important contribution to improving the processed surface quality, and are beneficial to improving tool's wear. The longitudinal-torsional ultrasonic vibration-assisted milling of titanium alloy thin-walled parts (LTCUVM) was proposed by Tong et al. [4], who showed that compared with CM, LTCUVM effectively reduces the average cutting force, reducing the surface roughness and chatter mark height. Rotary ultrasonic elliptical milling (RUEM) is a new ultrasonic vibration milling method for titanium alloys. However, the effect of this method on the microstructure of milled surfaces is not yet clear. Zhang et al. [5] comprehensively studied the surface characteristics and subsurface microstructure of titanium alloys; the results showed that, compared with the CM method, the surface micro-hardness of the RUEM method increased from 21.22 to 33.84%. Chen et al. [6] propose that ultrasonic vibration helical milling (UVHM) can reduce the axial cutting force by 38–64% compared with conventional helical milling. The drilling of composite materials still faces problems such as severe delamination and low efficiency [7]. Feng et al. [8, 9] established the prediction model of milling temperature and tool wear rate for ultrasonic vibration-assisted milling by experimenting ultrasonic vibration-assisted milling of aluminum alloys, which provides theoretical guidance for ultrasonic vibration-assisted milling. Wang et al. [10] proposed a new longitudinal and torsional coupled (LTC) vibration assisted drilling technology based on the conventional rotary ultrasonic drilling (Con-RUD); The cutting force generated by LTC-RUD is more than 50% less than Con-RUD. Yang et al. [11] established a model of the contact rate of abrasive particles and workpieces in ultrasonic vibration assisted grinding. Dong et al. [12] analyzed the edge-cutting mechanism of an ultrasonic vibration grinding hole exit through finite element simulation, provided theoretical guidance for the efficient and precise machining of small and deep holes in hard and brittle materials. Yu et al. [13] proposed an axial ultrasonic vibration assisted polishing method. By establishing a motion equation and trajectory simulation of abrasive particles in the polishing liquid, the effect of ultrasonic vibration on the polishing process was studied, and the results suggest that the addition of ultrasonic vibration effectively improves the polishing quality. Ultrasonic vibration assisted grinding is widely used to process of hard and brittle materials [14]. Shen et al. [15] found that during ultrasonic vibration assisted grinding (UVAG), because of the tiny cutting edge produced by ultrasonic vibration on diamond grits, the working surface of the diamond wheel maintains a stable grinding force and force ratio. It does not increase with the increase in material removal. Zhou, Yang and Feng et al. [11, 16, 17] analyzed the UVAG produces micro-deformed surfaces; Compared with conventional grinding, the surface

quality of the workpiece was effectively improved. Feng, Xiao and Li et al. [18–20] established different UVAG grinding force prediction models, and verified their reliability through experiments. Tool vibration frequency, tool vibration amplitude and speed are three important factors that affect ultrasonic vibration cutting (UVC) [21]. Kong et al. [22] studied in detail the influence of machining parameters on elliptical ultrasonic vibration cutting (EVC) through a finite element simulation. Guo and Lotfi et al. [23, 24] found that using EVC to produce micro-deformations on the surface of a workpiece is an advanced method for improving surface tribological performance. Tan et al. [25] used PCD tools to achieve ultra-precise sustainable machining of titanium alloys under UVC conditions. Through experiments and numerical simulations, Bai et al. [26] found that the average grain change size of UVC is smaller than that of conventional cutting (CC). Therefore, the damage degree of UAC is lower.

High material removal rate, low cutting force, and better surface finish are some advantages of high-speed machining (HSM) [27]. However, owing to the principles of EVC and UVC, traditional ultrasonic vibration cutting has a maximum vibration speed limit; thus, the advantages of this processing technology cannot be applied to HSM. Therefore, it is necessary to develop the high-speed vibration cutting (HVC) technology. The main contents of this paper are as follows: First, a model of high-speed vibration cutting is established, and the theoretical principle of tool/workpiece separation is analyzed. Second, high-speed vibration cutting involves precision cutting with smaller cutting depth and feed rate. The influence of the cutting edge radii on the experimental results can not be neglected. Furthermore, the accuracy of the finite element model was verified by comparing the experimental and simulation results. In addition, the effects of different cutting edge radii on the tool wear depth, cutting temperature, cutting force, and stress distribution in vibration cutting and traditional cutting were comprehensively studied. HVC, UVC, and CC were comprehensively discussed about tool wear, cutting force, and cutting temperature. Finally, the influence of two key parameters (vibration frequency and amplitude) on the cutting process in high-speed vibration cutting is studied.

2 The principle of high-speed vibration cutting

The traditional UVC and EVC tooltip movement trajectories are shown in Fig. 1. In UVC and EVC, because the direction of tool vibration is the same as the direction of the tool feed, the tool is periodically separated from the workpiece when the tool vibration speed is greater than the critical cutting speed, $V_C = 2\pi AF$, as shown in
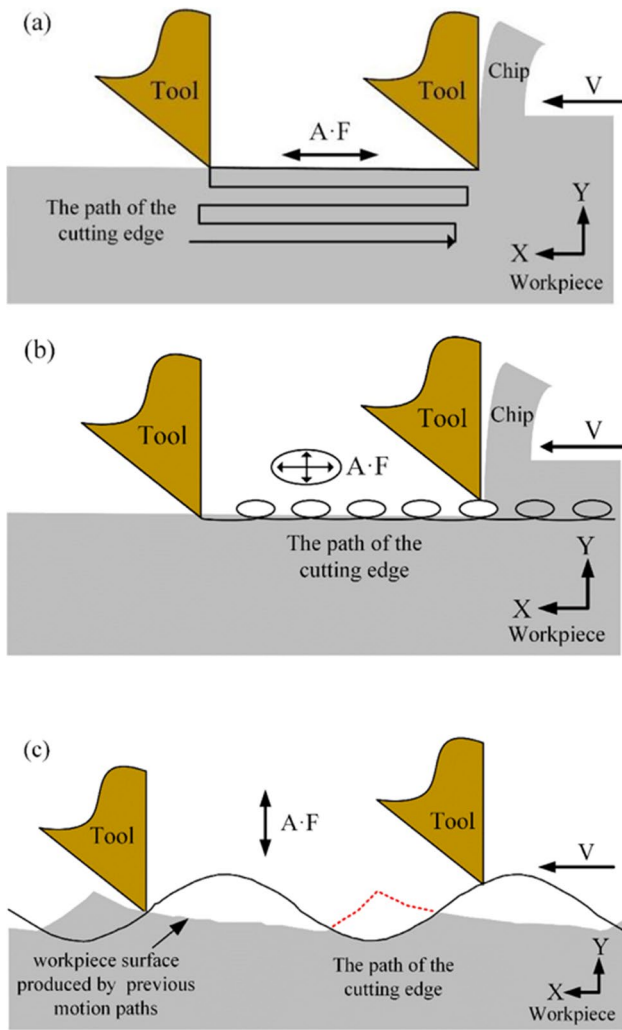
Fig. 1 Three kinds of vibration cutting processes: (**a**) UVC, (**b**) EVC, (**c**) HVC

Fig. 2 Schematic diagram of high-speed vibration cutting

$$V_x = 2\pi f_x A cos(2\pi f_x t + T_x) - v \qquad (3)$$

$$V_y = 2\pi f_x B cos(2\pi f_y t + T_y) \qquad (4)$$

The cutting temperature and cutting force are reduced, when the maximum V_c and V_x are more significant than the cutting speed v, and the cutting between the workpiece and the tool is interrupted.

The maximum tool vibration speeds of the UVC and EVC methods were calculated using the frequency and amplitude of the vibration. For example, when the frequency is 20000 Hz and the amplitude is 20 μm, the maximum vibration speed of the tool is approximately 2513 mm/s, and vibration cutting will not be invalid until the cutting speed is less than the maximum vibration speed. Therefore, high-speed vibration processing technology, which is no longer limited by the maximum tool vibration speed, is used in this section. In the HVC method, ultrasonic vibration causes the tool tip to vibrate perpendicular to the cutting speed to achieve interrupted cutting, and the tip and workpiece can still achieve intermittent cutting even if the cutting speed is very high, as shown in Fig. 1(c). Tool movement is considered the result of tool translation on the workpiece surface. Therefore, the calculated tool motion function is the same as the tool vibration function, and it can be expressed as [28]:

$$\begin{cases} z_v = A sin 2\pi F t \\ x_v = V_C t \end{cases} 0 \le t \le T \qquad (5)$$

where A is the vibration amplitude, F the vibration frequency, V_C the cutting speed and T the vibration period.

The high-speed vibration cutting process is illustrated in Fig. 2. The motion path of the tool relative to the workpiece can be described by establishing an $r - \theta - z$

Fig. 1(a). As shown in Fig. 1(b), the mechanism of elliptical ultrasonic vibration cutting is described. The vibration direction of the tool is elliptical along the X and Y directions, and its trajectory relative to the workpiece can be described as follows:

$$X_t = A sin(2\pi f_x t + T_x) - vt \qquad (1)$$

$$Y_t = B sin(2\pi f_y t + T_y) \qquad (2)$$

where A and B represent the amplitudes of the elliptical vibration in the X and Y directions, f_x and f_y are the vibration frequencies, t is the time, and T_X and T_y are the initial angles in the X and Y-directions, respectively. Deriving the derivatives of Eqs. (1), (2), the speed at which a tooltip is at a point in the elliptical trajectory relative to the workpiece can be expressed as follows:
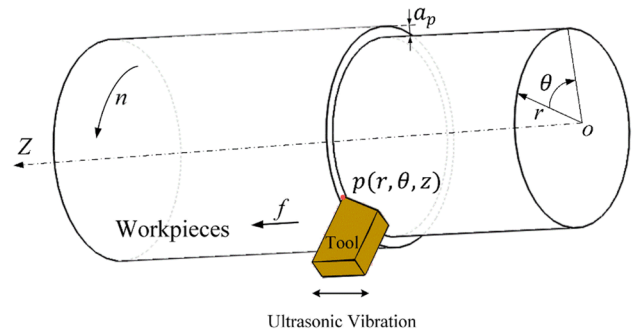
cylindrical coordinate system. The equation for random point p on the cutting edge in Fig. 2 can be expressed as follows:

$$\begin{cases} r = r_p \\ \theta = w_n t = \frac{n\pi}{30} t \\ z = A\sin(2\pi F t) + v_f t \end{cases} \tag{6}$$

where, r_p is the cutting radii of point p, mm; w_n is the angular velocity of the spindle, rad/s; n is the rotational speed of the spindle, r/min; v_f is the feed speed, mm/s; and f is the feed rate, mm/r. Subsequently z can be expressed as follow:

$$z = A\sin\left(\frac{60F}{n}\theta\right) + \frac{f}{2\pi}\theta \tag{7}$$

The cutting frequency ratio λ is defined as the ratio of the vibration frequency to the spindle speed, including the integer part K and fractional part ε, which can be expressed as:

$$\lambda = \frac{60F}{n} = K + \delta \tag{8}$$

The separation criteria of HVC are given by [28]:

$$\begin{cases} f \le 2A \\ \frac{\arcsin(f/2A)}{\pi} \le \delta \le \frac{\arcsin(f/2A)}{\pi} \end{cases} \tag{9}$$

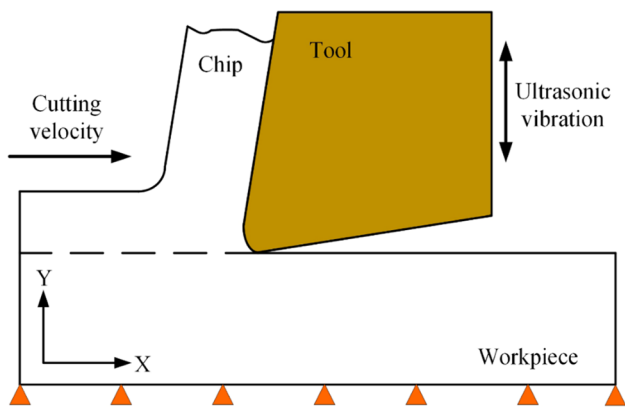## 3 Finite element model of HVC

The high-speed ultrasonic vibration assisted machining process of the titanium alloy was modeled using ABAQUS 2016, and the cutting process was simulated. A high-speed ultrasonic vibration orthogonal cutting diagram is shown in Fig. 3. The finite element simulation model adopts the updated Lagrange's finite adaptive meshing technique and element format. The workpiece was set as a plastic body, and the cutting tool was rigid. Both the tool and workpiece cell types are CPE4RT, the tool adopts a gradient mesh, the cell mesh at the tool tip is dense, the rest of the mesh is sparse, and the front and rear tool surfaces of the tool are divided into meshes by linear deviation. In order to improve the efficiency of the model operation, the mesh in the contact area between the tool and the workpiece is divided more densely, and the minimum mesh size is 1 μm. The workpiece is made of titanium alloy Ti-6Al-4 V, and its chemical composition is shown in Table 1. The height and length of the workpiece in the model are 0.02 mm and 0.5 mm, respectively. The bottom side of the workpiece has motion boundary conditions, and the top surface is a free surface.

Orthogonal cutting simulation of Ti6Al4V was carried out using an uncoated carbide (WC) tool (rake angle of 5°, clearance angle of 7°). Unlike the traditional cutting simulation, the direction of the tool vibration in the high-speed ultrasonic vibration cutting simulation is the direction of the feed speed instead of being fixed. To study the influence of vibration parameters and cutting edge radii on high-speed ultrasonic

Fig. 3 Simplified schematic diagram of boundary conditions for high-speed vibration cutting

Table 2 Finite element simulation of cutting parameters

Parameters	Values
Workpiece material	Titanium alloy Ti-6Al-4 V
Cutting tool material	Uncoated carbide cutting tool
Rake angle (deg)	5
Clearance angle (deg)	7
Cutting speed (m/min)	100, 150, 200, 300, 400
Vibration frequency (kHz)	20, 30, 40, 50
Vibration amplitude (μm)	4, 6, 8, 10
Uncut chip thickness (μm)	3
Cutting edge radius (μm)	1, 3, 5, 10

Table 1 The chemical composition of Ti6Al4V

Element	Al	V	Fe	O	Si	C	N	H	Others	Ti
%	5.5–6.8	3.5–4.5	0.3	0.2	0.15	0.1	0.05	0.01	0.5	Balance

vibration and traditional cutting more clearly, Table 2 lists the detailed cutting parameters. In the finite element simulation method, rapid and large deformation during high-speed cutting of metal materials causes element deformation that is difficult or even abnormal. In order to solve this difficulty, high-density meshing was performed in the primary deformation zone.

3.1 Material constitutive model

The material constitutive relation refers to a certain microstructure, flow stress, strain, and strain rate to the temperature thermodynamic state formed by the response. Therefore, in the process of simulating irreversible deformation, the material constitutive formula has a large impact on the accuracy of numerical simulation results. The Johnson-Cook material model was used to ensure the accuracy of the simulation results in the finite element model, and the physical properties of the workpiece material are listed in Table 3 [29].

Table 3 Johnson–Cook parameters for Ti-6Al-4 V alloy [30]

Property	Value
Yield stress A_0 (MPa)	968
Hardening modulus B (MPa)	380
Strain rate sensitivity $\dot{\varepsilon}$	0.0197
Hardening coefficient n	0.421
Thermal softening coefficient m	0.577
Reference strain rate $\dot{\varepsilon}_0$	0.1

$$\sigma = \left(A_0 + B\varepsilon^n\right)\left[1 + \mathrm{Cln}\left(\frac{\dot{\varepsilon}}{\dot{\varepsilon}_0}\right)\right]\left[1 - \left(\frac{T - T_r}{T_m - T_r}\right)^m\right] \quad (10)$$

where σ is the equivalent stress, A_0 is the initial yield stress, B is the hardening modulus, C is the strain rate dependency coefficient, ε is the plastic strain, $\dot{\varepsilon}$ is the strain rate, $\dot{\varepsilon}_0$ is the reference strain rate, T is the workpiece temperature, T_r is room temperature, T_m is the melting temperature, n is the strain hardening exponent and m is the thermal softening coefficient.

3.2 The frictional force

It is crucial to include the contact friction between the tool, workpiece, and chip to effectively analyze the friction in the cutting simulation. Tool friction in the HVC process is investigated in this section using a simplified intermittent machining model. As illustrated in Fig. 4(a), the tool has a downward velocity relative to the free surface at the top of the workpiece at the start of the cutting cycle (State I < t < II) and cuts from the bottom left of the workpiece. At this point, the tool friction is opposite to the direction of its movement. The tool begins to move towards the top surface of the workpiece from State II to State III. The tool friction direction was opposite to the chip flow direction, and the friction force did not affect the tool side. The tool and workpiece are in the separation period from state III to state IV; there is no cutting behavior in the entire stage, and the tool will not rub against the workpiece. It can be concluded that the direction of the frictional force of the tool changes once during the vibration cycle. Compared to traditional ultrasonic vibration cutting, the direction of the tool friction force changes

Fig. 4 Dynamic friction in high-speed vibration cutting

(a) State I<t<II

(b) State II<t<III

(c) State III<t<IV

(d) HVC cutting process
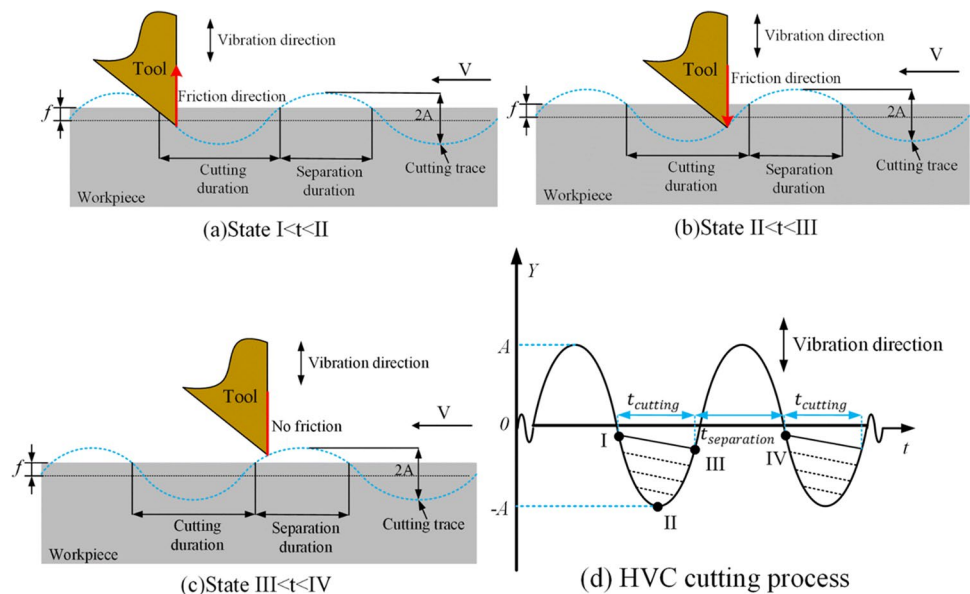
twice in one cycle [3]. In high-speed vibration cutting, the contact area between the tool and the workpiece is the shaded part of the peak in Fig. 4(d), which is smaller than the rectangular contact area of UVC or CC. High-speed vibration cutting contributes to lower friction by reducing the effective contact area between the tool and the workpiece, resulting in longer tool life.

3.3 The wear model

Tool wear is an essential criterion for determining tool failure. According to ISO standard 3685 (1993), tool failure is considered when tool wear meets the following standards:

1) Average flank wear VB = 0.2 mm
2) Maximum flank wear VBmax = 0.3 mm

For the first time, Yen et al. [30] came up with a tool wear prediction method based on the finite element method
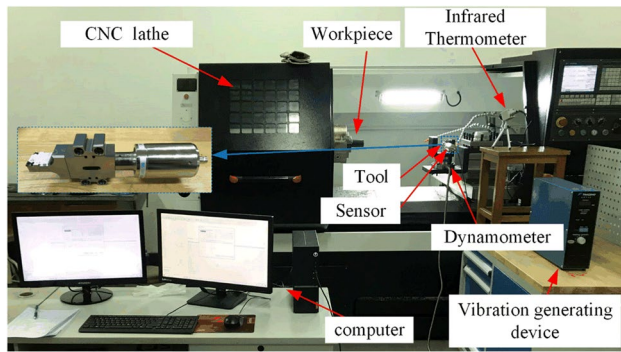
Fig. 5 The experiment platform of ultrasonic elliptical vibration cutting

simulation cutting for a two-dimensional model. In this study, the Usui wear model was used to predict tool wear in simulated cutting. Malakizadi et al. [31] compared experimental and simulation results to verify the reliability of the model. Based on the Usui tool wear model, the tool wear during the cutting of titanium alloys can be predicted by finite element simulation [32]. The Usui wear model can be expressed as:

$$w = \int apVe^{-b/T}dt \tag{11}$$

where p is the interface pressure, V is the sliding velocity, T is the interface temperature, dt is time increment, a and b are the experimentally calibrated coefficients.

3.4 Experimental validation

The ultrasonic vibration experimental device used in this study is illustrated in Fig. 5. The CNC lathe is a 980TC3-d lathe from Guangzhou CNC Company. The force gauge is a Kistler 9272 piezoelectric force gauge was used. The experiment used uncoated cemented carbide tools with a rake angle of 0° and relief angle of 11° produced by Japan's Mitsubishi Materials Co., Ltd. The model used was TPGX080204. The cutting condition was dry cutting, and the cutting fluid function of the machine tool was turned off. This experiment adopted the principle of a single variable and conducted nine sets of verification experiments. The three different cutting speeds are 400 mm/s a, 500 mm/s, and 600 mm/s; the three different feeds are 0.02 mm/rev, 0.03 mm/rev, and 0.04 mm/rev; and the depth of cutting are 0.02 mm, 0.03 mm, and 0.04 mm. The machining parameters of all simulation experiments were the same as those of the experiment and were

Fig. 6 Comparison of experimental cutting force and simulated cutting force

Fig. 7 Orthogonal cutting process diagram: (**a**) Macro-cutting, (**b**) Micro-cutting
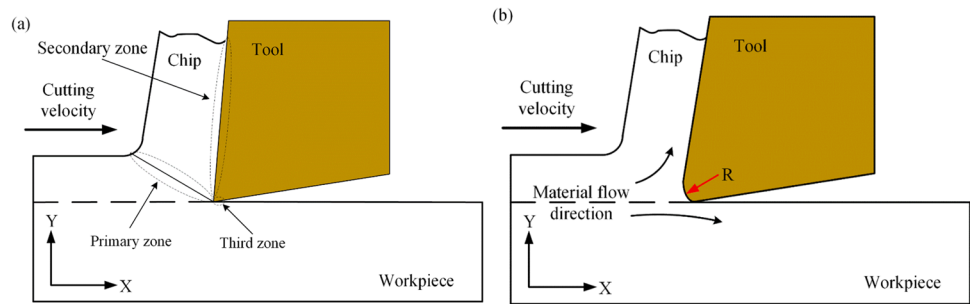
repeated at least twice under dry cutting conditions to obtain the final average value. Figure 6 shows the average values of the experimental and simulated cutting forces for different cutting parameters. As the cutting speed changed, the differences between the experimental and simulated cutting forces were 17%, 15%, and 16%, respectively. As the cutting depth changed, the differences between the experimental and simulated cutting forces for the three cutting depths were 11%, 6%, and 7%, respectively. With the feed rate change, the differences between the experimental and simulated cutting forces were 15%, 16%, and 9%, respectively. Since there are many factors affecting the cutting force in the actual experiment, such as tool wear during machining, and the simulation model only considers simple factors such as temperature, therefore the simulation value is always smaller than the experimental value. Under different cutting speeds, cutting depths, and feed rates, the simulation results agreed with the experimental results, which verified the accuracy of the finite element cutting model.

Fig. 8 Schematic diagram of the influence of minimum uncut chip thickness on chip formation

4 Results and discussions

High-speed vibration cutting is a precision machining method with low cutting depth. Therefore, the cutting edge of the tool is no longer considered sharp, and the influence of the edge radii cannot be ignored during processing. As shown in Fig. 7(a), the cutting edge is considered perfectly sharp during macro cutting because the thickness of the uncut chip is tens to hundreds of times the radii of the cutting edge. However, owing to the limitation of the cutting parameters, the cutting edge radii and thickness of the uncut chip are of the same order of magnitude in precision cutting, as shown in Fig. 7(b). Thus, the macro-cutting model is unsuitable for precision cutting. Therefore, cutting edge radii' influence was studied by this paper separately on the cutting process during CC and HVC.

4.1 The effect of cutting edge radii on CC

Whether chips are formed depends on the minimum uncut chip thickness, which is about 0.2–0.3 times the radii of
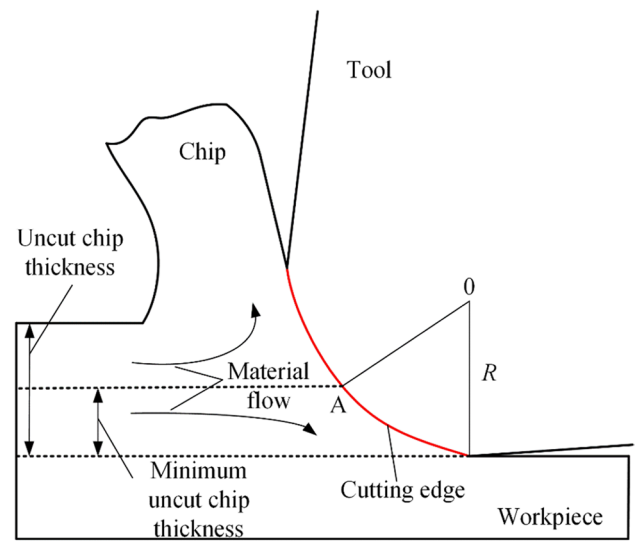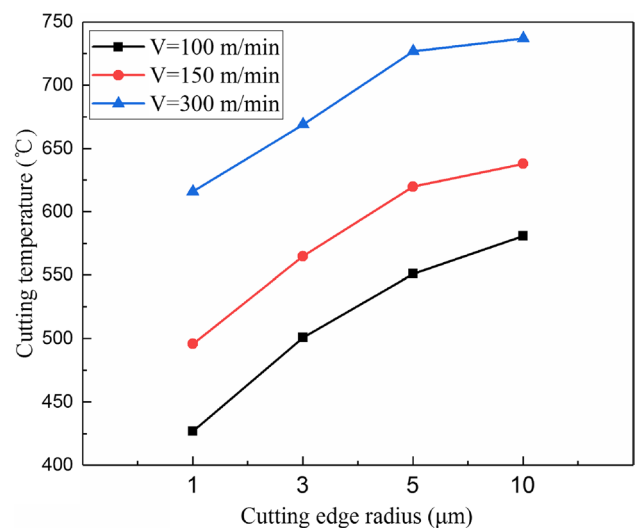

Fig. 9 Cutting temperature with different cutting speeds and cutting edge radius

cutting edge [33]. Point A was assumed to be on the cutting edge. Above this point, the material forming chips flowed out along the rake face, as shown in Fig. 8. Below this point, the material flows up, which is an elastic–plastic deformation without material removal. When the chip thickness remains unchanged, the degree of elastic–plastic deformation of the chip increases with the increase in chip radii, which leads to higher temperature and energy consumption [34]. The results of the simulation experiments shown in Fig. 9 confirm the authenticity of the analysis. The cutting temperature refers to the maximum temperature of the workpiece surface during cutting. When the other machining parameters remain unchanged, the cutting temperature increases as the cutting edge radii' increases. When the cutting edge radii were less than or slightly larger than the thickness of the uncut chip, the cutting edge radii had a more significant effect on the cutting temperature. Increasing the cutting edge radii did not significantly change the cutting temperature when the cutting edge radii were more significant than the uncut chip thickness. When the minimum uncut thickness is sufficiently large, the material's elastic–plastic deformation plays a dominant role in the cutting process. Therefore, the cutting edge radii change did not significantly increase the cutting temperature.

Figure 10 demonstrates how the average cutting force varies with the radii of the cutting edge at three different cutting speeds, which is similar to how the cutting force varies with cutting temperature. At the same cutting speed, the cutting force increases practically linearly as the cutting edge radii increase. The cutting force in precision cutting is made up of shearing and ploughing forces. The simulation software employs a shear friction model with the continuous shear
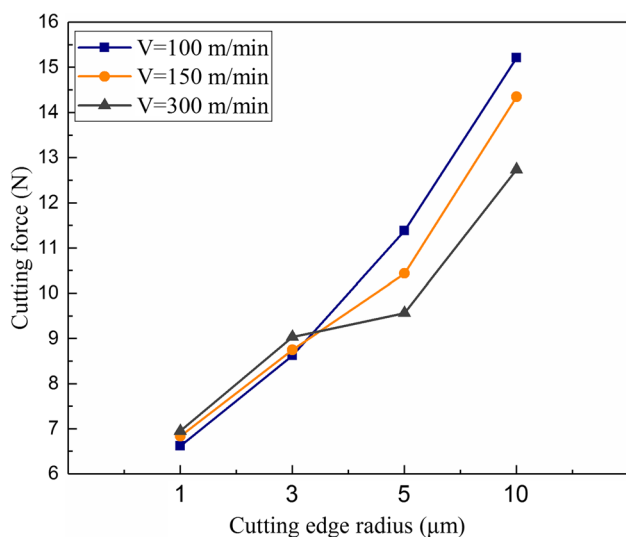
assumption, and the friction coefficient is set to 0.6. Ploughing force is generated in micro-cutting by the elastic–plastic deformation of the workpiece material caused by the cutting edge. The higher the cutting edge radii, the greater the minimum uncut thickness; the more materials processed on the cutting edge arc, the more serious the plowing process, and the larger the ploughing force, which leads to a linear increase in total cutting force.

In micro-cutting, flank wear is the main wear mode. In contrast, there was less wear on the rake face due to friction with the chips. The uncut chips were not significantly thicker than the minimal uncut thickness, which caused this wear pattern. In this cutting simulation experiment, the uncut chip thickness was approximately equal to the minimal thickness of the uncut chip. As shown in Fig. 11, when the cutting edge radii are less than the thickness of the uncut chip, the tool wear depth increases with the cutting edge radii. However, when the cutting speed was 150 m/min, and the cutting edge radii increased from 5 to 10 μm, the tool wear depth decreased.

The stress distribution of the workpiece is depicted in Fig. 12 around different cutting edge radii at a cutting speed is 150 m/min. When the cutting edge radii of the tool are much smaller than the uncut chip thickness in the cutting simulation, the material flows primarily out of the rake face to form chips. In this case, the ploughing phenomenon was still very slight, and the cutting force increased only slightly. As shown in Fig. 12(a), because the cutting edge radii are substantially smaller than the uncut chip radii, the material below the tooltip is limited from flowing upward, resulting in increased stress at the tooltip and the highest stress region concentrated at the front face and upper section of the cutting edge. As the radii of the cutting edge are close to the thickness of the uncut chip, the tooltip arc replaces the rake
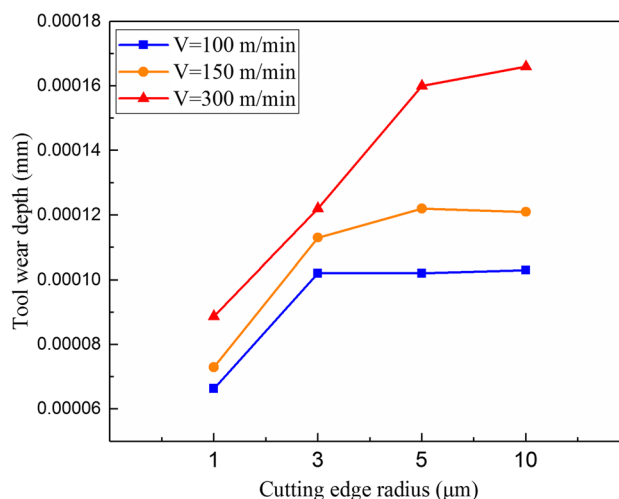

Fig. 10 Cutting force with different cutting speeds and cutting edge radius
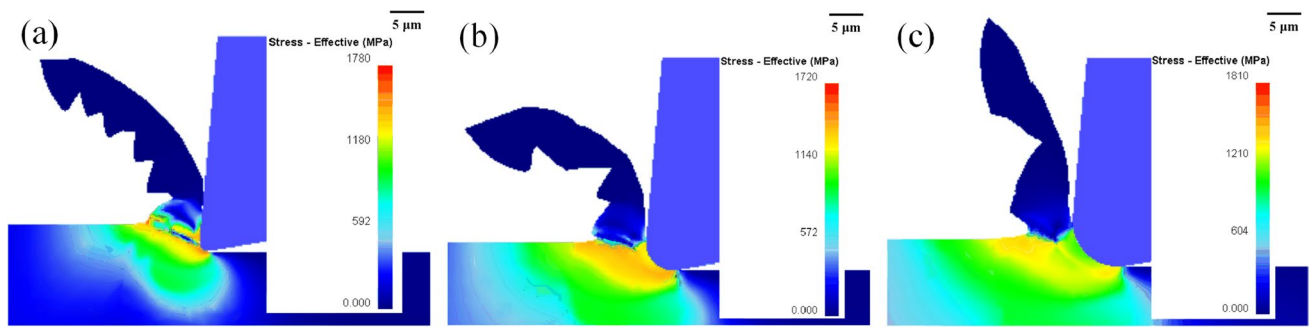

Fig. 11 Tool wear depth with different cutting speeds and cutting edge radius

Fig. 12 Stress distribution of different cutting edge radii: (**a**) $R = 1$ μm, (**b**) $R = 3$ μm, (**c**) $R = 5$ μm

face to cut the workpiece. Material flows out along the cutting edge arc above point A to form chips, and elastic–plastic deformation occurs along the cutting edge arc below point A. As shown in Fig. 8, the increase in the ploughing force significantly increased the total cutting force, and the maximum area stress was distributed around the cutting edge arc, as shown in Fig. 12(b). The difference in the cutting edge radii causes a difference in the position of point A as shown in Fig. 7. When the radii of the cutting edge are greater than the thickness of the uncut chip, only the arc at the bottom of the cutting edge cuts the workpiece, and the material at the lower part of the tooltip is restricted to a narrow region enclosed by the arc of the cutting edge and workpiece. Ploughting dominated the cutting process at this time, with the maximum stress zones placed at the bottom and sides of the cutting edge arc, as illustrated in Fig. 12(c).

4.2 The effect of cutting edge radii on HVC

The effect of different cutting edge radii on high-speed vibration cutting under the same cutting conditions was studied in this section (ultrasonic vibration frequency of 40 kHz, vibration amplitude of 5 μm, and cutting speeds of 100 m/min, 150 m/min, 200 m/min, 300 m/min, and 400 m/min). Figure 13 depicts the relationship between the tool wear depth and cutting edge radii for different cutting speeds and cutting modes. Compared with CC, UVC did not reduce the tool wear depth during high-speed cutting. Even at higher cutting speeds (V = 300 m/min, V = 400 m/min), the tool wear of the UVC was greater than that of the CC. This is because when the tool cutting direction is opposite to the vibration direction, the real cutting speed increases, generating more cutting heat and increasing the tool wear in the ultrasonic vibration cutting process. However, compared to CC, HVC significantly reduced the tool wear depth at different cutting speeds. For example, when the cutting edge radii was 3 μm and the cutting speed was 400 m/min, the wear of the CC tools was three times that of the HVC tools in Fig. 13(e). The real cutting thickness was greater than the set thickness of

the uncut chip because the tool traveled sinusoidally along the cutting speed direction; therefore, the micro-cutting model was modified and the influence of the radii on the cutting effect was minimized. As shown in Fig. 13, the tool wear curve became exceedingly smooth as the cutting edge radii increased during vibration cutting.

Figure 14 shows the cutting temperature at a cutting speed of 150 m/min. Under this cutting condition, the cutting speed is much greater than the maximum vibration speed of the tool (75.4 m/min). At this time, the intermittent cutting characteristics of the tool and workpiece of UVC disappear. However, when the tool vibration speed is opposite to the cutting speed, the actual cutting speed will be greatly increased and the cutting temperature will increase. Therefore, the cutting temperature of UVC is higher than HVC and CC when the cutting speed is too high. HVC will not cause the separation of workpiece and tool in vibration cutting to disappear due to the increase of cutting speed. However, in the cutting stage, the tool cuts down into the workpiece to increase the thickness of the uncut chips, and increase the cutting temperature. Under the condition of dry cutting, there is no significant difference in cutting temperature between high-speed vibration cutting and traditional cutting.

Vibration cutting was divided into cutting and separation times. In HVC cutting time, the cutting force was greater than CC because the tool moved sine perpendicular to the workpiece surface, but no cutting force or small cutting force was produced at the subsequent separation time. Therefore, as shown in Fig. 15, the difference in average cutting force between HVC and CC is relatively modest. However, when the separation time is too long, the average cutting force of HVC is less than that of CC, such as the cutting speed is 150 m/min. In CC, the curve of cutting force changing with cutting tip radii is steeper at the same cutting speed. During HVC, however, the change in the cutting route minimizes the impact of cutting edge radii on cutting force and gentles the curve.
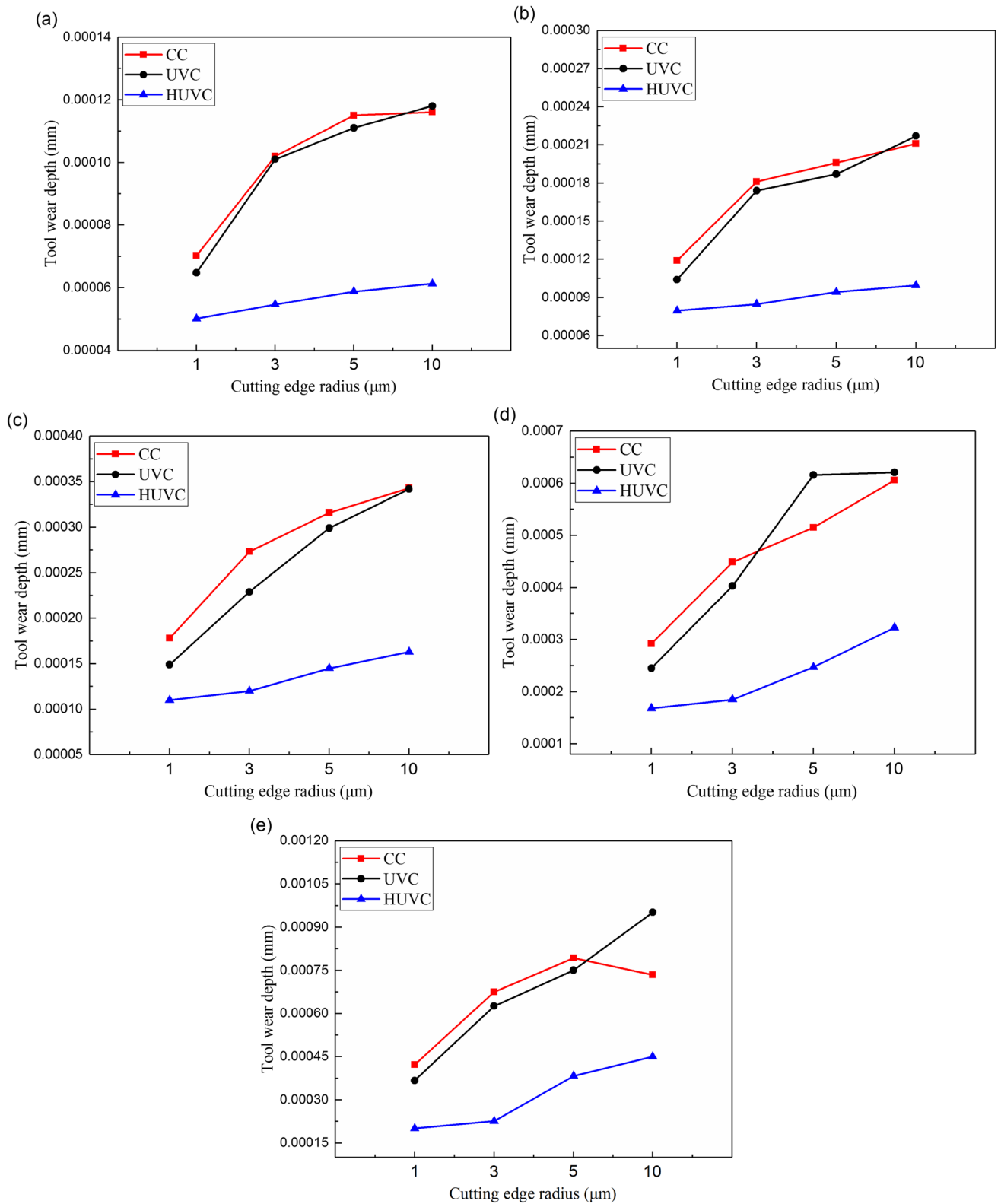
Fig. 13 Tool wear depth of different cutting methods: (**a**) $V = 100$ m/min, (**b**) $V = 150$ m/min, (**c**) $V = 200$ m/min, (**d**) $V = 300$ m/min, (**e**) $V = 400$ m/min
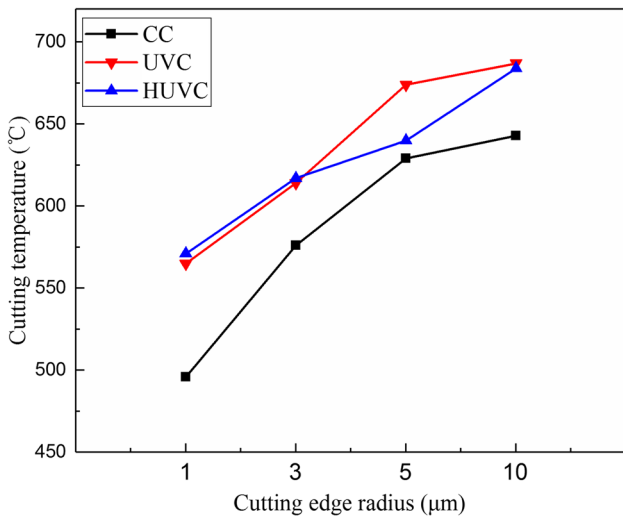
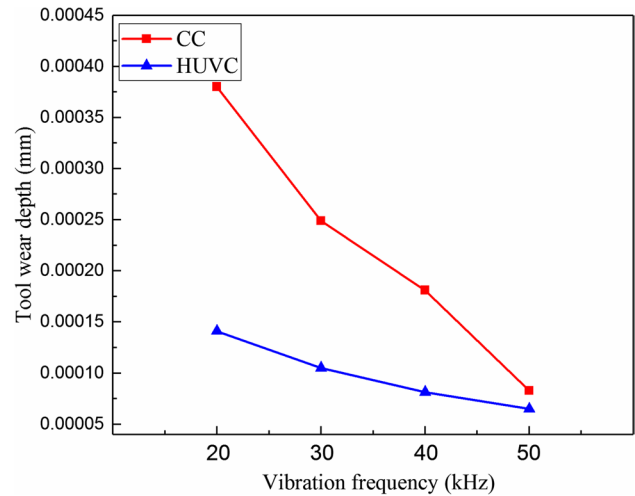**Fig. 14** Cutting temperature of different cutting methods

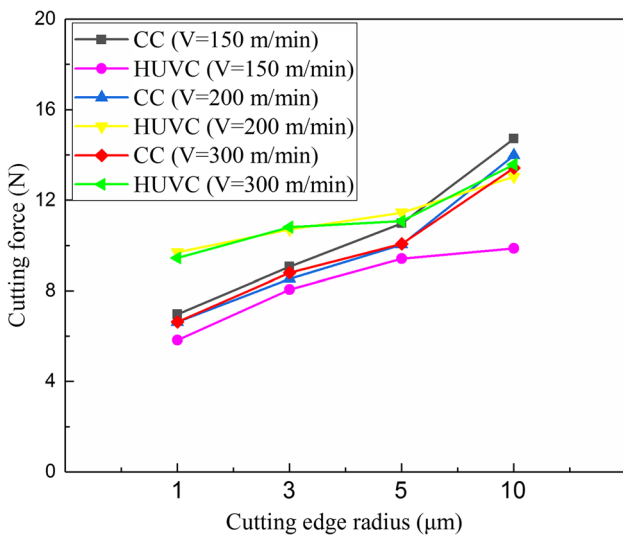**Fig. 16** Tool wear depth for different vibration frequencies

Fig. 15 Cutting force for different cutting speeds and different cutting methods

4.3 The effect of vibration frequency on HVC

Figure 16 shows the tool wear depth under different tool vibration frequencies (cutting edge radii of 3 μm, cutting speed of 150 m/min). The total cutting time was the time of one cycle for each vibration frequency. This is because if the same cutting time or cutting length is set to compare the total wear depth, the number of vibration cycles completed by tools with different vibration frequencies will be different for the same cutting time or cutting length. Therefore, it is difficult to compare the tool wear depth at different frequencies and the results are inaccurate. For example, when the total cutting time was set to 0.00015 s. The tool can complete

3 cycles of vibration motion at a vibration frequency of 20 kHz. However, when the vibration frequency is 50 kHz, the tool can complete 7.5 cycles of vibration motion. This 0.5 cycle did not realize separation of the workpiece and tool, which affected the reduction rate of the wear depth. It can be observed from Fig. 16 that the tool wear of conventional cutting is about 2.7 times of the tool wear when the vibration frequency is 20 kHz. However, as the vibration frequency increased, the tool wear reduction achieved by high-speed vibration cutting became increasingly weaker. With an increase in tool vibration frequency, the reduction in tool wear depth of high-speed vibration cutting decreases compared with traditional cutting. When the vibration frequency was 40 kHz, the wear depth of traditional cutting tools was about 2.23 times that of high-speed vibration cutting tools. Although the cutting speed was the same as that of traditional cutting, the cutting results produced when using high-speed vibration cutting methods were different. This is because the processing parameters were the same but the material removal rates of traditional cutting and high-speed vibration cutting are different. The material removal rate η can be expressed as follows:

$$\eta = 1000 \cdot fa_p V_c \tag{12}$$

The difference between the material removal rate Eq of traditional cutting is that the cutting speed obtained using the high-speed ultrasonic vibration method is not the actual cutting speed. After vibration is applied to the tool, the set cutting speed becomes the actual cutting speed V_{hc}. At this time, the expression for the material removal rate becomes:
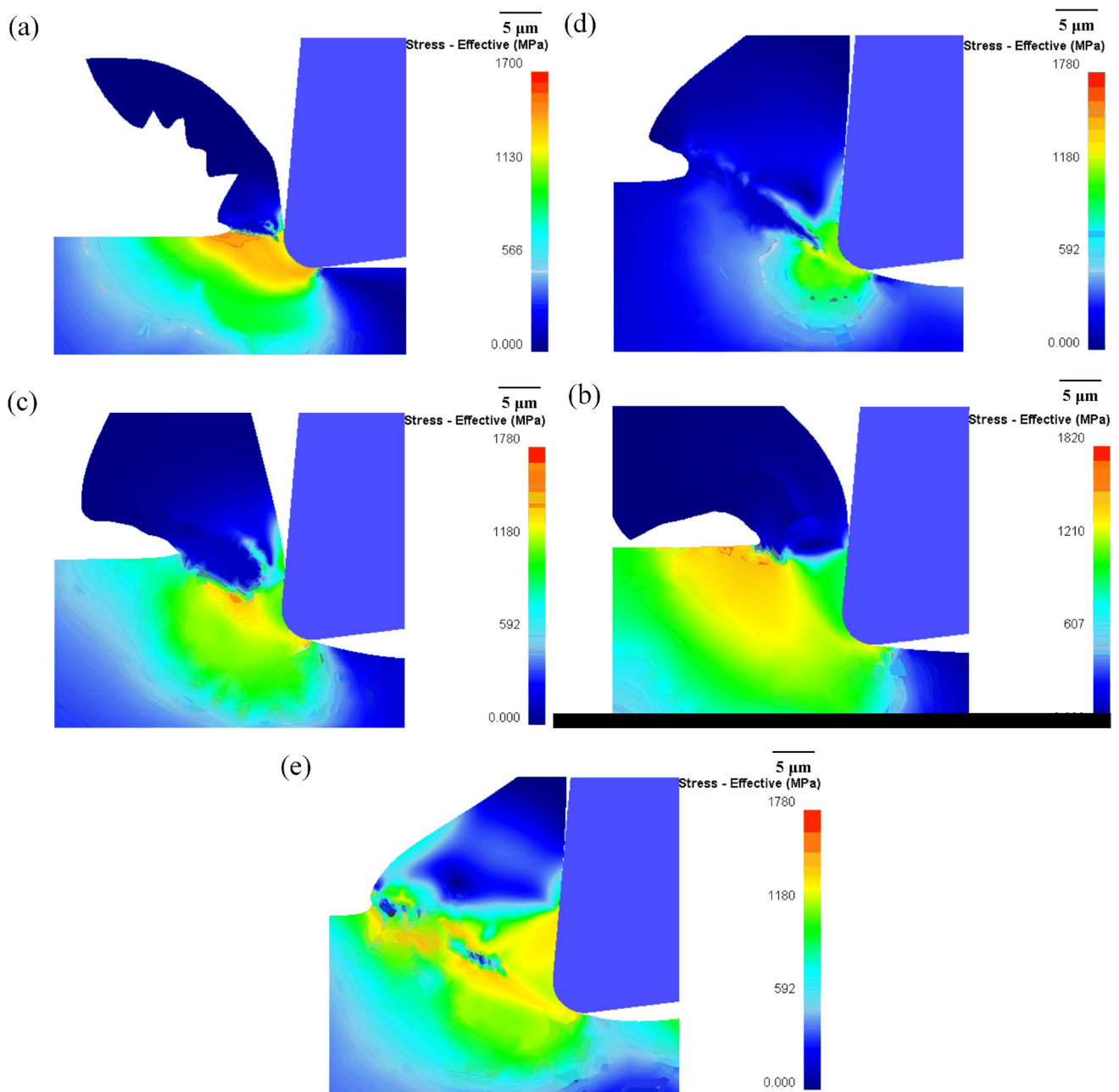
$$\eta_{hc} = 1000 \cdot fa_p V_{hc} \tag{13}$$

Fig. 17 Stress distribution under different vibration frequencies: (**a**) $F = 0$ kHz, (**b**) $F = 20$ kHz, (**c**) $F = 30$ kHz, (**d**) $F = 40$ kHz, (**e**) $F = 50$ kHz

The actual cutting speed of high-speed vibration cutting increased as the vibration frequency increased. High-speed vibration cutting can reduce tool wear during high-speed cutting; however, as the vibration frequency increases, the tool removes more workpiece material than in traditional cutting. This weakens the ability of the high-speed ultrasonic vibration to reduce tool wear during high-speed cutting.

The stress distributions generated by cutting the work-piece at different vibration frequencies are shown in Fig. 17. As shown in Fig. 17, the maximum stresses generated by the different vibration frequencies and traditional cutting

were almost the same. When the vibration frequency was 20 kHz, there was no significant difference between the high-stress distribution areas of high-speed vibration cutting and traditional cutting. As the vibration frequency increased from 20 to 40 kHz, the high stress distribution area generated by vibration cutting continued to decrease, as shown in Fig. 17(b–d). However, the high stress distribution area does not always decrease with an increase in vibration frequency. As can be seen from Fig. 17(d, e), When the vibration frequency was 50 kHz, the stress increased and the area of the high stress distribution area also increased. This
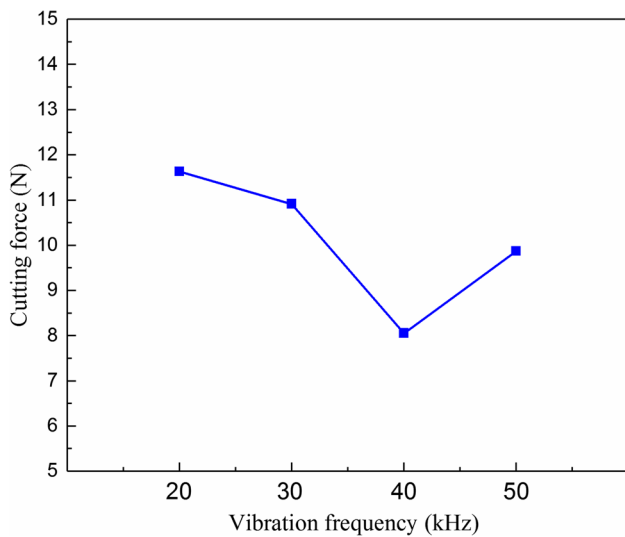
Fig. 18 Cutting force for different vibration frequencies

4.4 The effect of vibration amplitude on HVC

The tool wear depths at different vibration frequencies and cutting speeds are shown in Fig. 19. When the vibration amplitude was 0 μm, it means that the cutting method was traditional cutting and no vibration was applied to the tool. A vibration amplitude of less than the uncut chip thickness was not considered in the cutting simulation as shown in Fig. 18. This is because the vibration amplitude is an important factor in high-speed vibration cutting to achieve tool/workpiece separation. According to a previous theoretical analysis, when the vibration amplitude is smaller than the uncut chip thickness, the tool and workpiece cannot be separated. The same vibration amplitude and different cutting speeds had different effects on reducing tool wear. When the cutting speed was 150 m/min, the high-speed vibration cutting method reduced tool wear the most when the vibration amplitude was 4 μm. As the vibration amplitude increased, tool wear depth decreased. However, when the cutting speed was 300 m/min, the wear depth of the tool reduced by the high-speed vibration cutting method increased with an increase in the vibration amplitude. When the vibration amplitude increased from 4 to 8 μm, the reduction in tool wear depth reached a maximum. Later, the increase in the vibration amplitude led to an increase in the depth of the tool wear.

The high-speed vibration cutting method performed well in reducing tool wear during high-speed cutting. However, under dry cutting conditions, compared with traditional cutting, this method has no obvious effect on reducing the cutting temperature and even slightly increases the cutting temperature [35]. The effect of the vibration amplitude on the cutting temperature for high-speed vibration cutting of the titanium alloy is shown in Fig. 20. It can be seen from Fig. 20

phenomenon is related to the cutting force during high-speed vibration cutting. Figure 18 shows the average cutting force under different vibration frequency conditions. The average cutting force of the vibration cutting first decreases and then increases as the vibration frequency increases. The cutting force was lowered to a minimum when the vibration frequency increased from 20 to 40 kHz. At this time, the stress value and distribution range were the smallest. Subsequently, the cutting force increased and the stress value and distribution range increased.
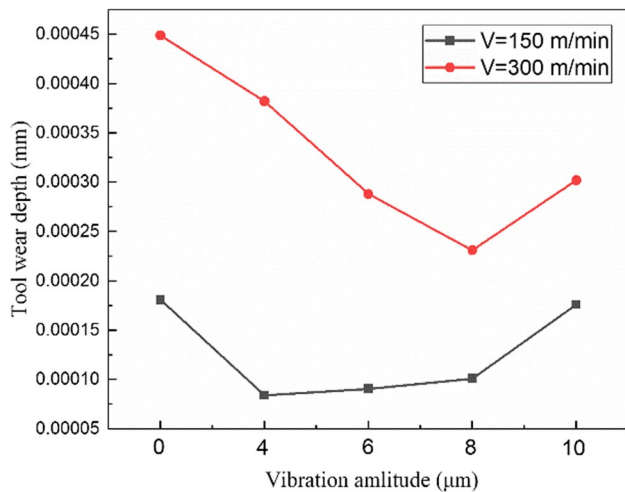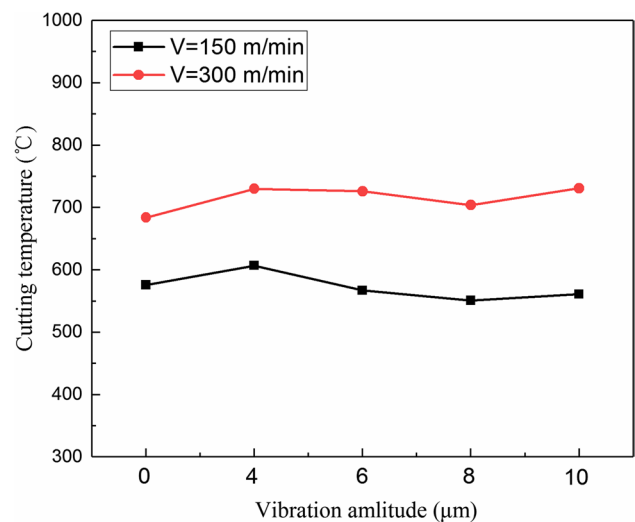

Fig. 19 Tool wear depth for different vibration amplitudes

Fig. 20 Cutting temperature for different vibration amplitudes

that the cutting temperature of high-speed vibration cutting is almost the same as that of traditional cutting no matter the cutting speed is 150 m/min or 300 m/min. With a change in the vibration amplitude, the cutting temperature exhibits a small change. When the cutting speed was 150 m/min, the cutting temperature decreased slightly as the vibration amplitude increased. At a cutting speed of 300 m/min, the cutting temperature did not always decrease as the amplitude increased. The cutting temperature was the lowest when the amplitude was 8 μm. This can be explained by the fact that as the vibration amplitude increases, the actual material removal rate of vibratory cutting continues to increase, which generates more cutting heat and increases the cutting temperature.

Figure 21 shows that the stress distribution area of the workpiece changes as the vibration amplitude changes. The stress distribution area in the workpiece was reduced owing to the introduction of the vibration cutting method. The maximum stress values of traditional cutting and vibration cutting did not change significantly. In traditional cutting,

the high stress distribution area in the workpiece is the largest. This is because in the cutting process, the workpiece material first undergoes elastic deformation; if the load is removed before reaching the elastic deformation limit, the strain returns to zero. Otherwise, plastic deformation occurred. As the vibration amplitude increased from 4 to 6 μm, the separation of the tool and workpiece became more obvious, and the area of stress distribution in the workpiece was reduced. As the vibration amplitude increases from 6 to 8 μm, the cutting force increases and the elastic deformation becomes significant, and the high stress distribution area becomes larger.

5 Conclusions

In this study, titanium alloy was machined by conventional cutting, ultrasonic vibration cutting, and high-speed vibration cutting using cutting tools with different cutting
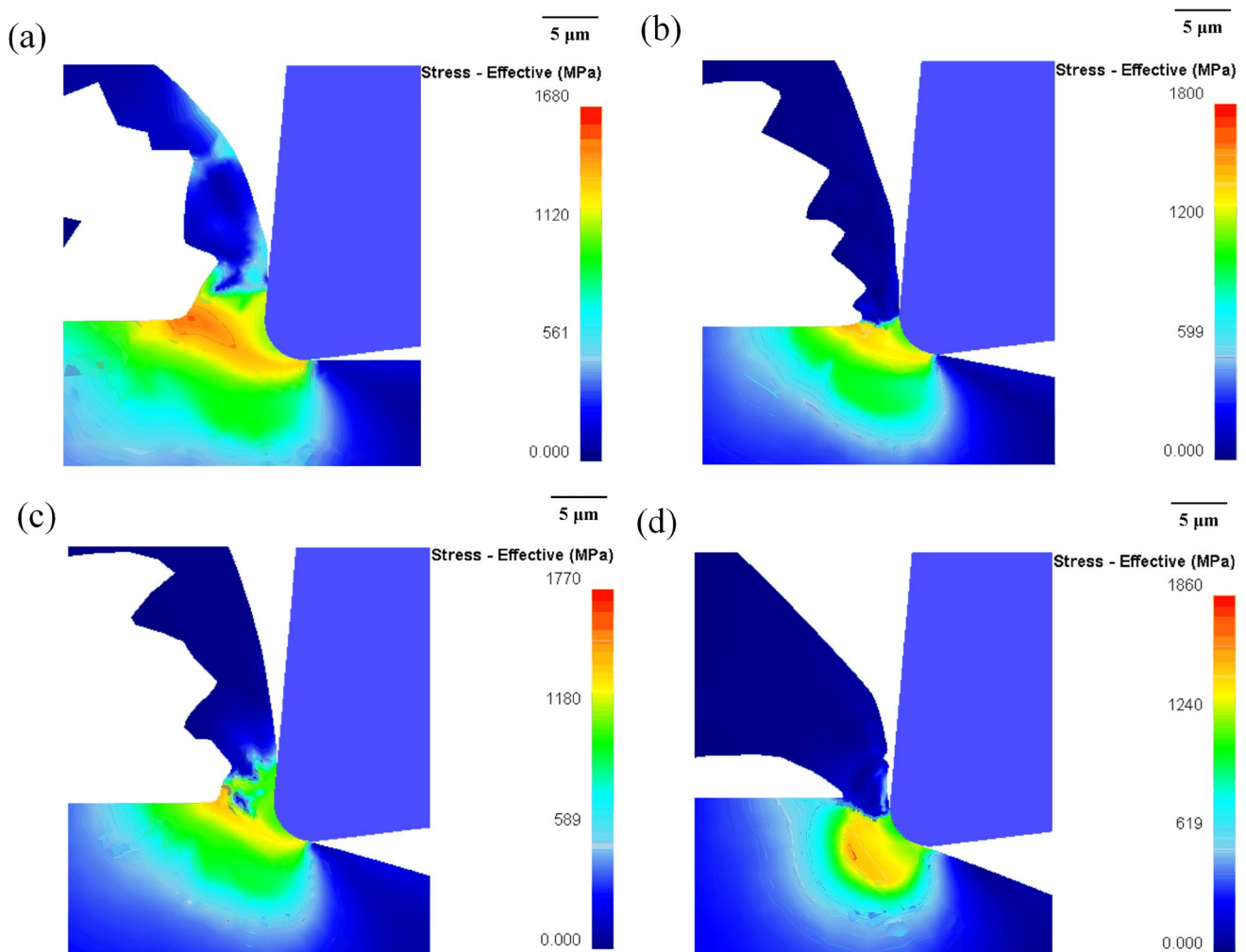

Fig. 21 Stress distribution under different vibration amplitudes: (**a**) $A = 4$ μm, (**b**) $A = 6$ μm, (**c**) $A = 8$ μm, (**d**) $A = 10$ μm

edge radii. Several critical conclusions were obtained and addressed as follows:

1. The vibration direction of the high-speed vibration cutting technology is perpendicular to the direction of the cutting speed. This feature overcomes the limitation that traditional ultrasonic vibration cutting existence of the maximum vibration speed. The tool wear of traditional cutting in high-speed cutting of titanium alloy is 1–3 times that of high-speed vibration cutting tool wear. However, the cutting temperature of high-speed vibration cutting without lubrication is not significantly different from that of traditional cutting. When the cutting speed is much higher than the maximum vibration speed of ultrasonic vibration cutting, ultrasonic vibration cutting produces a higher cutting temperature and deeper tool wear depth than traditional cutting.

2. In precision machining, the cutting edge radii of the tool and uncut chip thickness are of the same order of magnitude. The minimum uncut chip thickness determines whether chips are formed; thus, the cutting edge radii have a significant impact on the cutting process. When the cutting edge radii is smaller than the uncut chip thickness, the material below the tooltip is limited from flowing upward, resulting in an increased stress at the tooltip and the highest stress region concentrated at the front face and upper section of the cutting edge, the cutting force, cutting temperature and tool wear increase as the cutting edge radii increases. However, when the cutting edge radii is much larger than the uncut chip thickness, the arc at the bottom of the cutting edge cuts the workpiece, ploughting dominates the cutting process at this time, increasing the cutting edge radii having a smaller effect on tool wear. Furthermore, high-speed vibration cutting changes the path of the tool movement, enhances the actual material removal rate, and weakens the impact of the cutting edge radii on the cutting process.

3. Two important parameters of vibration cutting, vibration amplitude and vibration frequency, have different effects on cutting results. As the vibration frequency increases from 20 to 50 kHz, the value of high-speed vibration cutting to reduce tool wear has decreased. When the vibration frequency is 20 kHz, the tool life of high-speed vibration cutting is 2.7 times that of the traditional cutting. As the vibration frequency increases to 40 kHz, the tool life of high-speed vibration cutting is only 2.23 times that of the traditional cutting. When the cutting speed is 300 m/min, as the vibration amplitude increases, the decrease in tool wear depth first increases and then decreases. When the vibration amplitude is 8 μm, the tool wear is reduced the most. When the cutting speed is 150 m/min, the tool wear becomes more and more serious as the vibration amplitude increases.

Declarations

References

1. Zhu L, Ni C, Yang Z, Liu C (2019) Investigations of micro-textured surface gener-ation mechanism and tribological properties in ultrasonic vibration-assisted milling of Ti–6-Al–4V. Precis Eng 57:229–243. https://doi.org/10.1016/j.precisioneng.2019.04.010

2. Zheng K, Liao W, Dong Q, Sun L (2018) Friction and wear on titanium alloy surface machined by ultrasonic vibration-assisted milling. J Braz Soc Mech Sci Eng 40(9):1–12. https://doi.org/10.1007/s40430-018-1336-9

3. Ni C, Zhu L, Yang Z (2019) Comparative investigation of tool wear mechanism and corresponding machined surface characterization in feed-direction ultrasonic vibration assisted milling of Ti–6Al–4V from dynamic view. Wear 436:203006. https://doi.org/10.1016/j.wear.2019.203006

4. Tong J, Wei G, Zhao L, Wang X, Ma J (2018) Surface microstructure of titanium alloy thin-walled parts at ultrasonic vibration-assisted milling. Int J Adv Manuf Technol. https://doi.org/10.1007/s00170-018-3005-7

5. Zhang M, Zhang D, Geng D, Liu J, Shao Z, Jiang X (2020) Surface and sub-surface analysis of rotary ultrasonic elliptical end milling of Ti-6Al-4V. Mater Des 191:108658. https://doi.org/10.1016/j.matdes.2020.108658

6. Chen G, Ren C, Zou Y, Qin X, Lu L, Li S (2019) Mechanism for material removal in ultrasonic vibration helical milling of Ti6Al4V alloy. Int J Mach Tools Manuf 138:1–13. https://doi.org/10.1016/j.ijmachtools.2018.11.001

7. Xing Y, Deng J, Zhang G, Wu Z, Wu F (2017) Assessment in drilling of C/C-SiC composites using brazed diamond drills. J Manuf Process 26:31–43. https://doi.org/10.1016/j.jmapro.2017.01.006

8. Feng Y, Hsu FC, Lu YT, Lin YF, Lin CT, Lin CF, Lu YC, Liang SY (2020) Temperature prediction of ultrasonic vibration-assisted milling. Ultrasonics 108:106212. https://doi.org/10.1016/j.ultras.2020.106212

9. Feng Y, Hsu FC, Lu YT, Lin YF, Lin CT, Lin CF, Lu YC, Liang SY (2020) Tool wear rate prediction in ultrasonic vibration-assisted milling. Mach Sci Technol 24(5):758–780. https://doi.org/10.1080/10910344.2020.1752240

10. Wang J, Feng P, Zhang J, Guo P (2018) Reducing cutting force in rotary ultrasonic drilling of ceramic matrix composites with longitudinal-torsional coupled vibration. Manuf Lett 18:1–5. https://doi.org/10.1016/j.ijmachtools.2013.11.003

11. Yang Z, Zhu L, Ni C, Ning J (2019) Investigation of surface topography formation mechanism based on abrasive-workpiece contact rate model in tangential ultrasonic vibration-assisted CBN grinding of ZrO2 ceramics. Int J Mech Sci 155:66–82. https://doi.org/10.1016/j.ijmecsci.2019.02.031

12. Dong G, Lang C, Li C, Zhang L (2020) Formation mechanism and modelling of exit edge-chipping during ultrasonic vibration grinding of deep-small holes of microcrystall-ine-mica ceramics. Ceram Int 46(8):12458–12469. https://doi.org/10.1016/j.ceramint.2020.02.008

13. Yu T, Guo X, Wang Z, Xu P, Zhao J (2019) Effects of the ultrasonic vibration field on polishing process of nickel-based alloy Inconel718. J Mater Process Technol 273:116228. https://doi.org/10.1016/j.jmatprotec.2019.05.009

14. Wang Y, Lin B, Wang S, Cao X (2014) Study on the system matching of ultrasonic vibration assisted grinding for hard and brittle materials processing. Int J Mach Tools Manuf 77:66–73. https://doi.org/10.1016/j.ijmachtools.2013.11.003

15. Shen JY, Wang JQ, Jiang B, Xu XP (2015) Study on wear of diamond wheel in ultrasonic vibration-assisted grinding ceramic. Wear 332:788–793. https://doi.org/10.1016/j.wear.2015.02.047

16. Zhou W, Tang J, Chen H, Shao W (2019) A comprehensive investigation of surface generation and material removal characteristics in ultrasonic vibration assisted grinding. Int J Mech Sci 156:14–30. https://doi.org/10.1016/j.ijmecsci.2019.03.026

17. Feng Y, Hsu FC, Lu YT, Lin YF, Lin CT, Lin CF, Lu YC, Liang SY (2020) Surface roughness prediction in ultrasonic vibration-assisted milling. J Adv Mech Des Syst Manuf 14(4):JAMDSM0063–JAMDSM0063

18. Li C, Zhang F, Meng B, Liu L, Rao X (2017) Material removal mechanism and grinding force modelling of ultrasonic vibration assisted grinding for SiC ceramics. Ceram Int 43(3):2981–2993. https://doi.org/10.1016/j.ceramint.2016.11.066

19. Xiao X, Zheng K, Liao W, Meng H (2016) Study on cutting force model in ultrasonic vibration assisted side grinding of zirconia ceramics. Int J Mach Tools Manuf 104:58–67. https://doi.org/10.1016/j.ijmachtools.2016.01.004

20. Feng Y, Hsu FC, Lu YT, Lin YF, Lin CT, Lin CF, Lu YC, Liang SY (2020) Force prediction in ultrasonic vibration-assisted milling. Mach Sci Technol 25(2):307–330. https://doi.org/10.1080/10910344.2020.1815048

21. Nath C, Rahman M (2008) Effect of machining parameters in ultrasonic vibration cutting. Int J Mach Tools Manuf 48(9):965–974. https://doi.org/10.1016/j.ijmachtools.2008.01.013

22. Kong C, Wang D (2018) Numerical investigation of the performance of elliptical vibration cutting in machining of AISI 1045 steel. Int J Adv Manuf Technol 98(1):715–727. https://doi.org/10.1007/s00170-018-2277-2

23. Guo P, Ehmann KF (2013) An analysis of the surface generation mechanics of the elliptical vibration texturing process. Int J Mach Tools Manuf 64:85–95. https://doi.org/10.1016/j.ijmachtools.2012.08.003

24. Lotfi M, Sajjady SA, Amini S (2019) Wettability analysis of titanium alloy in 3D elliptical ultrasonic assisted turning. Int J Light Mater Manuf 2(3):235–240. https://doi.org/10.1016/j.ijlmm.2019.05.001

25. Tan R, Zhao X, Guo S, Zou X, He Y, Geng Y, Hu ZJ, Sun T (2020) Sustainable production of dry-ultra-precision machining of Ti–6Al–4V alloy using PCD tool under ultrasonic elliptical vibration-assisted cutting. J Clean Prod 248:119254. https://doi.org/10.1016/j.jclepro.2019.119254

26. Bai W, Sun R, Leopold J, Silberschmidt VV (2017) Microstructural evolution of Ti6Al4V in ultrasonically assisted cutting: numerical modelling and experimental analysis. Ultrasonics 78:70–82. https://doi.org/10.1016/j.ultras.2017.03.005

27. Tan DW, Guo WM, Wang HJ, Lin HT, Wang CY (2018) Cutting performance and wear mechanism of TiB2-B4C ceramic cutting tools in high speed turning of Ti6Al4V alloy. Ceram Int 44(13):15495–15502. https://doi.org/10.1016/j.ceramint.2018.05.209

28. Sui H, Zhang X, Zhang D, Jiang X, Wu R (2017) Feasibility study of high-speed ultrasonic vibration cutting titanium alloy. J Mater Process Technol 247:111–120. https://doi.org/10.1016/j.jmatprotec.2017.03.017

29. Mishra SK, Ghosh S, Aravindan S (2018) 3D finite element investigations on textured tools with different geometrical shapes for dry machining of titanium alloys. Int J Mech Sci 141:424–449. https://doi.org/10.1016/j.ijmecsci.2018.04.011

30. Yen YC, Söhner J, Lilly B, Altan T (2004) Estimation of tool wear in orthogonal cutting using the finite element analysis. J Mater Process Technol 146(1):82–91. https://doi.org/10.1016/S0924-0136(03)00847-1

31. Malakizadi A, Gruber H, Sadik I, Nyborg L (2016) An FEM-based approach for tool wear estimation in machining. Wear 368:10–24. https://doi.org/10.1016/j.wear.2016.08.007

32. Liu X, Zhang X, Wang D (2020) Numerical analysis of different cutting edge radii in hot micro-cutting of Inconel 718. Proc Inst Mech Eng C J Mech Eng Sci 234(1):196–210. https://doi.org/10.1007/s13369-020-05034-z

33. Lai X, Li H, Li C, Lin Z, Ni J (2008) Modelling and analysis of micro scale milling considering size effect, micro cutter edge radius and minimum chip thickness. Int J Mach Tools Manuf 48(1):1–14. https://doi.org/10.1016/j.ijmachtools.2007.08.011

34. Liu X, DeVor RE, Kapoor SG (2006) An analytical model for the prediction of minimum chip thickness in micromachining. J Manuf Sci Eng 128(2):474–481. https://doi.org/10.1115/1.2162905

35. Zhang X, Lu Z, Peng Z, Sui H, Zhang D (2018) Development of a tool-workpie-ce thermocouple system for comparative study of the cutting temperature when high-speed ultrasonic vibration cutting Ti-6Al-4V alloys with and without cutting fluids. Int J Adv Manuf Technol 96(1):237–246. https://doi.org/10.1007/s00170-018-1600-2